INL/RPT-22-67519

High-Temperature Creep Test Suite for Grizzly

May 2022

G. Singh[1]
M. Messner[2]
L. Munday[1]
B. W. Spencer[1]

[1]Idaho National Laboratory
[2]Argonne National Laboratory

INL is a U.S. Department of Energy National Laboratory
operated by Batelle Energy Alliance, LLC

INL/RPT-22-67519

High-Temperature Creep Test Suite for Grizzly

G. Singh[1]

M. Messner[2]

L. Munday[1]

B. W. Spencer[1]

[1]**Idaho National Laboratory**
[2]**Argonne National Laboratory**

May 2022

Idaho National Laboratory
Computational Mechanics and Materials
Idaho Falls, Idaho 83415

http://www.inl.gov

Prepared for the
U.S. Department of Energy
Office of Nuclear Energy
Under DOE Idaho Operations Office
Contract DE-AC07-05ID14517

Page intentionally left blank

ABSTRACT

A recent development in Grizzly has focused on improving its ability to model the high-temperature response of alloys, enabling its use for the predictive modeling of material response for advanced reactor applications. This report documents an effort to expand the example and assessment test suites in Grizzly to include a set of problems that exercise the models for the high-temperature response of components relevant to advanced reactors. These problems can be used to assess the accuracy of models, provide examples for users interested in modeling this class of problems, monitor performance on large-scale problems, and use as test cases for future feature development.

CONTENTS

1 INTRODUCTION

Grizzly is a code for simulating aging processes and their effects on nuclear power plant components and structures [1]. Early efforts focused on light water reactors (LWRs), with an emphasis on reactor pressure vessels and concrete structures, both of which are potentially life-limiting nuclear power plant components because of the extreme difficulty of repair or replacement. More recently, the emphasis of Grizzly development has shifted to issues surrounding the behavior of structural components in advanced reactors, a variety of which are currently under development.

One of the major differences between the advanced reactors being pursued and current LWRs is that many of the advanced reactors are designed to operate at significantly higher temperatures. While the coolant in an LWR is typically around 300 °C, significantly higher temperatures are targeted for advanced reactors, ranging from around 300 °C to as high as 1000 °C depending on the reactor type [2]. Predicting the long-term performance of alloy components operating in these high-temperature environments is critical for advanced reactor development. To meet this need, researchers have been developing a simulation capability for such components in the last couple of years [3, 4]. Two major classes of constitutive models they are developing and integrating into Grizzly are phenomenological models based on fitting of model parameters to experimental data and reduced-order models based on the response of a mesoscale model that can be applied for engineering-scale simulations.

To ensure that these capabilities perform adequately for the class of problems they are intended for, it is important that suites of practical test cases representative of the target applications be developed in conjunction with the code development. The open-source Multiphysics Object-Oriented Simulation Environment (MOOSE) framework [5] that Grizzly is based on provides an environment for automated testing [6] for multiple classes of test problems. Each MOOSE-based application generally has a large suite of regression tests that ensure that the accepted behavior of the code is maintained when changes are made. These tests exercise various combinations of capabilities in the code. These test are very effective at ensuring that components of the code behave as intended, and are important for quality assurance. The full set of regression tests is run for each proposed code change, so by necessity, these are relatively small, fast-running problems. One of the objectives for these problems is that they should run in less than 2 seconds each, which severely limits the size of the models.

Because of these constraints on the size of the regression tests, they are generally not representative of the actual types of problems that the MOOSE-based applications are targeting, which are generally large-scale, long-running models that would be impractical to run every time a change is proposed to the code. It is essential to ensure that the codes can reliably run these large-scale problems and that the accuracy and performance is maintained over time as changes are made to the code.

The Bison code has long had suites of large-scale example and assessment problems [7, 8]. The assessment problems consist of validation problems, in which results are compared against experimental data, as well as benchmark problems, where the code is compared against solutions from other codes, and verification problems, where simulation results are compared with analytical solutions of problems relevant to the class of problems being solved by the code. The same testing environment provided by MOOSE for running regression tests is applied to these large-scale problems and works with the queuing systems used on high-performance computing clusters. Rather than running these problems with every change request for the code, these problems are run on a nightly and weekly basis, depending on the size of the models, with larger models only being run weekly. In a similar manner, sets of assessment and example problems have been developed recently for Grizzly [9, 10]. These have included problems relevant for LWR reactor pressure vessel integrity and concrete structure performance.

The work documented here expanded the example and assessment test suites in Grizzly to include a set of problems that exercise the models for the high-temperature response of components relevant to advanced reactors. The objectives of these test suites are similar to those described for the other test suites. In cases where experimental component-scale data is available, these can be used to assess model accuracy. They can be used to provide examples for users interested in modeling this class of problems. They are also important for quantifying and monitoring trends in performance on large-scale problems over time and as test cases for future feature development.

The problems in these test suites exercise a number of important foundational capabilities in the code, including advanced constitutive models, as well as a variety of capabilities relevant to this class of problem in the finite element code that those models are run within.

The test suites currently include:

- Nozzle-to-Sphere Vessel Problem: This is a 304 stainless-steel component built and tested at Oak Ridge National Laboratory (ORNL) described in Section 3.1.
- Hot Gas Duct Problem: This case is two concentric Alloy 617 tubes designed for a hot gas duct representative of what would be used in a high-temperature gas-cooled reactor described in detail in Section 3.2.
- Lateral Pipe Branch Problem: This is a representative lateral junction between a smaller and a larger Grade 91 pipe described in detail in Section 3.3
- Header Problem: This is a representative Grade 91 heat recovery steam generator outlet header described in detail in Section 3.4.
- End Plate Problem: This is a representative Grade 91 end plate at the transition between a larger and smaller diameter pipe described in detail in Section 3.5.
- Uniaxial Creep Tests: This is a set of problems simulating the uniaxial creep response of a set of materials of interest for high-temperature applications is described in Section 3.6.

2 MODELING FEATURES EXERCISED

This section describes a brief summary of the modeling features exercised by these test cases. These are not necessarily used by all of the problems but are used as noted in the individual cases.

2.1 Constitutive Models

Currently, the constitutive models in Grizzly for high-temperature alloy response are provided by the Nuclear Engineering Material model Library (NEML) [11] developed by Argonne National Laboratory. NEML provides a platform for defining and combining individual components of a constitutive model, such as a yield surface, flow rule, and hardening rule into a single usable model, and has been used as a basis for defining phenomenological models based on empirical observations for the major alloys currently of interest for high-temperature nuclear applications.

While the MOOSE TensorMechanics module provides a similar extensible framework for constitutive modeling, NEML currently provides a much richer set of models specifically targeted at high-temperature applications and thus is the basis for this work.

While the test suite is currently set up to operate using NEML-based models, an additional set of constitutive models known as the Los Alamos Reduced Order Models for Advanced Nonlinear Constitutive Equations (LAROMANCE) are under development and planned for integration with Grizzly in the near future. The LAROMANCE models are surrogate models (SMs) fit to the results from mesoscale polycrystal models and designed to be used at the engineering scale. By being based on mesoscale models that capture essential behavior, these models offer the potential for improved accuracy in a wider range of conditions than traditional empirically based models. While the current test suite does not exercise the LAROMANCE models, one of the test cases in this report (the Grade 91 header) was run using this model to demonstrate how this test suite can be used to evaluate new features as they are developed.

Brief descriptions of the constitutive models exercised in this test suite are provided below.

2.1.1 304 Stainless Steel

The secondary creep strain rate for 304 stainless steel is expressed as:

$$\dot{\epsilon}_m = A_o \left[\sinh\left(\frac{\beta_e \sigma}{n_e}\right)\right]^{n_e} \exp\left(-\frac{Q}{RT}\right) \tag{1}$$

where σ is the applied stress, Q is the activation energy, R is the gas constant, T is the temperature, and A, β_e, and n_e are fitting parameters [12]. At high stresses, Equation 1 reduces to an exponential stress-dependence form shown in Equation 2. The parameter values used for this model with 304 stainless steel are shown in Table 1.

$$\dot{\epsilon}_m = A_o \exp\left(-\frac{Q}{RT}\right) \exp\left(\beta_e \sigma\right) \tag{2}$$

Parameter	Value
A_o (%hr^{-1})	1.38 x 10^{13}
Q (cal/mol)	67,000
R (cal/mol-K)	1.987
β_e MPa^{-1}	$0.052967761 - 0.0001090393286\,T$
n_e	6

Table 1: Parameter values for NEML 304 stainless steel material creep model [13].

2.1.2 Grade 91

Details on the unified elasto-viscoplastic Grade 91 material model implemented in NEML are given in References [11] [14]. This material model was developed for uniaxial conditions but is extended to three dimensional stress and strain states using the Prandtl-Reuss flow rules.

The NEML elasto-viscoplastic Grade 91 model is a phenomenological model based on small strain theory where the total strain rate is composed of an elastic and viscoplastic component. The elastic response is given by the temperature dependent Young's modulus and Poisson's ratio, E and ν, given in Table 2. The viscoplastic strain rate follows a Perzyna flow rule [15] [14] with damage,

$$\dot{\epsilon}_{vp} = \left\langle \frac{\frac{\sigma}{1-\omega} - \sigma_0 - R}{\eta} \right\rangle^n \tag{3}$$

where $\langle\rangle$ are the Macaulay brackets, the viscoplastic parameter σ_0 is the yield stress, n is the rate sensitivity exponent, η is the viscosity, the damage variable is given by ω, and the hardening variable, R, uses the Voce hardening law [16]

$$R = Q\left[1 - \exp\left(-b|\epsilon_{vp}(t)|\right)\right] \tag{4}$$

where Q and b are hardening parameters. The viscoelastic strain rate given by Equation 3 is suitable for long-term monotonic loading and was developed for design analyses, such as the primary load design in the American Society of Mechanical Engineers (ASME) Boiler and Pressure Vessel Code. Chakraborty and Messner [14] used a Bayesian Markov Chain Monte Carlo analysis to fit distributions of viscoplastic parameters in Equation 3 to a range of Grade 91 experimental data. In this work, we use the mean values from their distributions fit to data for 550 °C, given in Table 2. The damage rate, $\dot{\omega}$, in Equation 3 is given by Leckie and Hayhurst [17] as

$$\dot{\omega} = \left(\frac{\sigma}{A}\right)^{\zeta} (1-\omega)^{-\phi} \tag{5}$$

where values for the adjustable damage parameters A, ζ, and ϕ, given in Table 2, are obtained from a linear Larson-Miller fit [14].

A LAROMANCE SM for Grade 91 alloy (P91, specifically) was also tested on one of the problems in the test suite. Data for the SM is created from a mechanistic-based crystal plasticity (CP) constitutive model [18] based on the Visco-Plastic Self-Consistent (VPSC) framework. The CP model was developed to capture physics-based thermal creep in Fe-Cr alloys. Inelastic deformation is captured through the evolution of mobile (cell) and immobile (wall) dislocations and their interaction with carbo-nitride precipitates (MX). Dislocations are able to bypass precipitates through thermally activated glide (Orowan looping) or non-conservative climb-assisted glide. This CP model was shown to capture experimentally observed temperature and stress-dependent primary and secondary creep rates and strains in Fe-Cr-Mo steel [19].

The SM is derived from a database of polycrystal simulations using the CP model in the VPSC framework, see Reference [20] for details. The synthetic database contains homogenized creep responses of Fe-Cr alloys

parameter	550 °C	600 °C
E (MPa)	174e3	168e3
ν	0.31	0.31
n	11.09	8.45
η	832.4	750.6
σ_0 (MPa)	3.769	3.547
Q (MPa)	106.9	112.6
b	47.99	44.0
A (MPa)	517	650
ζ	12.5	10
ϕ	2.5	2.0

Table 2: Mean values for NEML Grade 91 material model parameter distributions given by Chakraborty and Messner [14]. Units are MPa, mm, s.

for a range of inelastic strains, stresses, temperatures, and microstructures as reflected by the MX phase content and densities of wall (ρ_{wall}) and cell dislocations (ρ_{cell}). The SM uses internal state variables to explicitly link the evolution of cell and wall dislocation densities to the engineering-scale flow stress. The accumulated von Mises effective strain, ϵ_{vm}, captures the history-dependent strain hardening. A Prandlt-Reuss flow rule is used to provide an isotropic associative flow rule based on the von Mises stress. The SM uses polynomial regression to fit an orthogonal basis of Legendre polynomials to the synthetic database generated by the CP model. Results using this SM are in close agreement to VPSC results [20]. Parameter ranges and values used for these simulations are given in Table 3. The elastic response of the LAROMANCE P91 model uses the NEML parameters from Table 2. The LAROMANCE simulations use a material time-step limit based on the maximum change per time step in inelastic strain = 10^-4 , cell dislocation density = 10,000, and wall dislocation density = 10,000. Substepping is also enabled for the inelastic strain with a substep strain tolerance of 10^-4, note that the sub-stepping parameter is a tolerance and not the size of the inelastic strain increment. The material time stepping predicted two orders in magnitude larger time steps than were used in the simulations. Determining optimal material time stepping tolerances will be the focus of future work.

Parameter	Value	Range
Cell Dislocation Density (10^{12}m^{-2})	4.0	[1, 7]
Wall Dislocation Density (10^{12}m^{-2})	10.0	[6, 18]
MX Phase Fraction (ϕ_{MX})	0.008	[0.006, 0.02]
Model Limits	Header Simulation Max	Range
von Mises Stress (MPa)	67	[1, 150]
Effective Creep Strain (m/m) 0.0015	[0.0, 0.08]	
Temperature (°C)	600	[507, 627]

Table 3: LAROMANCE material model parameters and limits of modeling regime for Grade P91.

2.1.3 Alloy 617

Details on the creep and viscoplastic models for Alloy 617 (A617), as implemented in NEML, are given in References [13] and [21]. The A617 model assumes an additive decomposition of the elastic, plastic, and creep strains. The creep model is based on the Kocks-Mecking model [22, 23], and the creep strain rate (hrs^{-1}) is expressed in Equation 6.

$$\dot{\bar{\varepsilon}}_c = \dot{\epsilon}_o \exp\left(\frac{B\mu b^3}{AkT}\right)\left(\frac{\sigma}{\mu}\right)^{\frac{-\mu b^3}{AkT}} \tag{6}$$

where μ is the shear modulus, b a Burger vector, k the Boltzmann constant, T the temperature in Kelvin, σ the applied stress, and the parameters $\dot{\epsilon}_o$, A, and B are constants.

Parameter	Value
$\dot{\epsilon}_o$ (hrs^{-1})	1.657 x 10^7
A	-4.480
B	-2.510 for $T \leq 775$°C
B	-3.174 for $T > 775$°C
b (mm)	2.019 x 10^{-7}
k (mJ/K)	1.38064 x 10^{-20}

Table 4: Parameter values for creep model for NEML A617 [13].

2.1.4 316H Stainless Steel

The NEML model for 316H stainless steel was only used for the material comparison study described in subsection 3.6. The details of the model for 316H steel can be found in Reference [24].

2.1.5 Grade 22 Steel

As for the 316H steel, the NEML model for Grade 22 steel was also used only for the material comparison study described in subsection 3.6. The details of the model for this material are given in Reference [25].

2.2 Finite-Element Solution Features

Grizzly has access to the full set of features provided by the MOOSE framework it is based on, as well as the MOOSE modules it uses, of which "TensorMechanics" is the one that provides the capabilities exercised in this test suite. Some of the notable features used are summarized here.

2.2.1 Solvers

MOOSE relies on the Portable Extensible Toolkit for Scientific Computation (PETSc) library [26] for nonlinear equation solutions. PETSc can use a variety of techniques for the equation solution. MOOSE multiphysics problems are typically solved using a single nonlinear system of equations. It can be difficult to analytically form the Jacobian matrix for such problems, so one of the techniques commonly employed in MOOSE analyses is the preconditioned Jacobian-free Newton Krylov (PJFNK) method. This is a Newton-type technique in which the iterative update to the nonlinear solution is formed through a linear solution and a finite-difference procedure and does not require the Jacobian for the iterative solution update to be computed, although an approximation of the Jacobian is required for preconditioning. PETSc also provides a standard Newton method, which requires a more accurate Jacobian than PJFNK for good convergence.

A variety of preconditioning methods can be used within PETSc, with the most common packages employed for mechanics problems being SuperLU [27] and BoomerAMG [28]. SuperLU is a parallel

direct solver, while BoomerAMG is a algebraic multigrid preconditioner. While direct solvers such as SuperLU generally give the best convergence of the nonlinear system in terms of iteration counts, the general experience with MOOSE applications has been that they are limited to moderate-sized problems using less than about 200 central processing units (CPUs) because of high memory requirements. Iterative solvers such as BoomerAMG offer much better scalability and lower memory requirements than direct solvers, which is necessary for solving very large problems.

The general experience for mechanics problems in MOOSE has typically been that they run much better with direct solvers rather than iterative solvers and that PJFNK needs to be used, rather than the standard Newton method. In particular, problems with constraints, such as those involving contact, have been a particular challenge for iterative solvers because the algebraic multigrid methods tend to coarsen out degrees of freedom involved with constraints, which can severely deteriorate solution performance. However, some recent developments in MOOSE, such as the automatic scaling of the residuals, and continual improvements to the Jacobian provided by the mechanics models have allowed the standard Newton method with BoomerAMG to be used with very good convergence rates on some of the problems in this test suite, even with constraints. Other models still require the use of PJFNK with a direct solver, which works very effectively on these problems but has higher memory demands and is not as scalable as iterative solvers.

2.2.2 Predictors

Many of the problems of interest for high-temperature component response involve tracking the slow evolution of creep-induced deformation under steady-state conditions. The solutions for problems of this type are often very close to that achieved by extrapolating the difference between the solutions from the previous two steps to the current step in the time discretization used in the finite-element model.

By default, MOOSE uses the solution from the previous solution time as the starting point for the nonlinear iterations in the current time. This is reasonable for problems that can have large changes in the nature of the loading from one step to the next. For problems with monotonically varying loading or response, however, using an extrapolation from the previous solutions can provide an improved estimate of the solution. To take advantage of this type of knowledge of the system behavior, MOOSE provides a "Predictor" system, which allows for a variety of custom-developed predictors to be used. The "SimplePredictor," which is a simple scaled extrapolation from the previous two converged solutions, is used for most of the test cases here and generally performs very well. Providing an initial guess close to the converged solution can significantly reduce the required iterations, and in many cases in this test suite, the initial guess is close enough to the solution that it meets the convergence criterion. As a result, in those steps no solution iterations are required, although an option is used to force at least one nonlinear iteration.

2.2.3 Coordinate Systems

The test suite consists of a mixture of problems that are axially symmetric (i.e., geometries formed by rotating a body about an axis of symmetry) and those that are inherently three-dimensional (3D). MOOSE provides foundational support for axisymmetric representations, and the standard set of formulations in the TensorMechanics module have full support for two-dimensional (2D) axisymmetric modeling. If their behavior can be treated as that of an infinite cylinder, some simple pipe geometries, which are also of interest for high-temperature applications, can also be represented using one-dimensional (1D) axisymmetric models if the right constraints are applied, and the axisymmetric models in TensorMechanics support 1D in addition to 2D axial symmetry. This permits the use of very small, efficient models to capture the essential aspects of the model behavior.

2.3 Boundary Conditions and Constraints

As is common for mechanics problems, the problems in this test suite all employ standard Dirichlet boundary conditions (BCs) at various locations in the model. These problems generally all involve pressured pipes or vessels, and the displacements of the end of a pipe or plane through a vessel are fixed in one direction using Dirichlet BCs. In the current set of models, the planes where such BCs are applied all align with the Cartesian axes, but if there were a need for such BCs, an option is available in TensorMechanics through the recently developed "PenaltyInclinedNoDisplacementBC." Fixed displacements are also imposed in some cases at specific nodes to prevent the zero-energy modes that would result from unrestrained rigid body motion of the body. Most of these models also impose pressure boundary conditions, which are applied normal to the element facets on the surface of interest, and are a standard feature of TensorMechanics. For the models that require solving for a temperature field, Dirichlet BCs are also applied to account for temperature changes during the start, shutdown, and accident conditions.

A common issue that arises in modeling pressurized pipes or components connected to pipes that continue past the region of interest included in the model is the handling of the free ends of those pipes. In many applications, those free ends are connected to a long section of pipe that should be treated as closed, so the pressure load should be balanced with an axial load applied to the end of the component, and that end of the component should be forced to remain planar while still allowing free expansion. The pressure applied to obtain the correct axial tensile stress is applied on pipes' end to simulate the loads generated by the internal pressure in the pipes in axial direction. This applied pressure stress is given as:

$$\sigma_{axial} = P\left(\frac{r_i^2}{r_o^2 - r_i^2}\right) \tag{7}$$

where P is the internal pressure and r_i and r_o are the inner and outer radii of the pipe, respectively. There are two ways of ensuring that the sections remain planar in Grizzly currently, as outlined below.

For higher dimensional models (including 2D axisymmetric and 3D), a negative pressure that balances out the integrated load caused by the pressure over the pipe cross section is applied to the cut face of the pipe. To keep the cut surface planar, a constraint called the "EqualValueBoundaryConstraint" can be applied to keep one component of the displacement equal across the whole cut surface. This can be used in conjunction with the pressure BC and gives the desired behavior if the pipe is aligned in the Cartesian direction. It is possible to omit the constraint, which will give inaccurate results near the free surface but acceptable ones some distance away from the free surface.

For 1D axisymmetric models, the x-direction is the radial direction and the y-direction is the axial direction. Infinite cylinder conditions are imposed by using a generalized plane strain condition in the y-direction, which permits nonzero strains in the y-direction but forces the strains in the y-direction to be equal across the model. Pressure loads can also be imposed in the y-direction within this system.

2.4 Material-Based Time Stepping and Substepping

The efficient and accurate solution of the class of problems studied here is highly dependent on the size of the time step taken. While the nonlinear solver can successfully obtain solutions with large time steps, these steps may introduce unacceptably large errors in the integration of the incremental inelastic response at local material points. Two fairly recently developed capabilities in MOOSE are helpful for addressing this issue: material-based time stepping and substepping. These are currently used in a subset of these problems, but their usage will be expanded as this test suite is further developed.

The material-based time stepping control in MOOSE allows an arbitrary postprocessor (a MOOSE object that computes a single scalar value from the solution) to control the size of the next time step and another mechanism based on a "Terminator" object to force the time step to be cut if the current time step is too large. The material models used here can compute a maximum time step based on an allowable inelastic strain increment, and the Postprocessor used to govern the time step is computed by taking the minimum value of that material time step. This mechanism is used on some of these problems to ensure that the time step is neither too large (resulting in inaccurate solutions) or too small (resulting in excessive computation time).

Substepping permits the material models running at locations in the model with the highest strain increments to split the current step into multiple substeps. This allows the global model to run at a relatively large time step but ensures adequate solution accuracy in regions where the strain is rapidly evolving. This technique is especially effective in problems with strong strain localization in certain regions of the model.

3 EXAMPLES AND ASSESSMENT CASES

3.1 Nozzle-to-Sphere Vessel Problem

The nozzle-to-sphere vessel assessment case is based on one of the experimental tests conducted at ORNL as part of a United States Department of Energy program to develop the elevated-temperature structural design methodology for liquid-metal and other advanced reactors [29].

3.1.1 Geometry Mesh and Material

For this validation case, a 2D axisymmetric finite element model was analyzed. The dimensions of the test specimen are shown in Figure 1. The meshed model is shown in Figure 2. The meshed model consist of 3,282 QUAD8 elements (Exodus II format) [30]. Since the ORNL tests were performed on a 304 stainless steel component, we used a NEML model calibrated for that alloy for the analysis. The creep model used for this material is described in section 2.

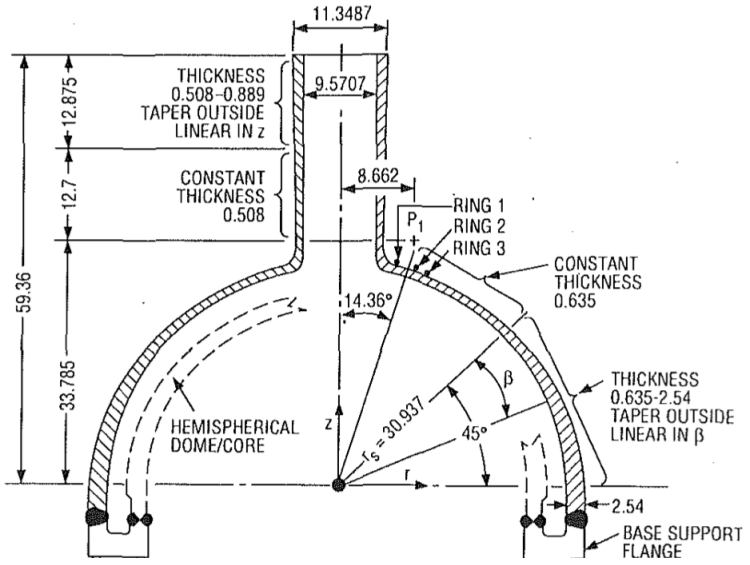

Figure 1: Dimensions of the ORNL nozzle-to-sphere vessel [29].

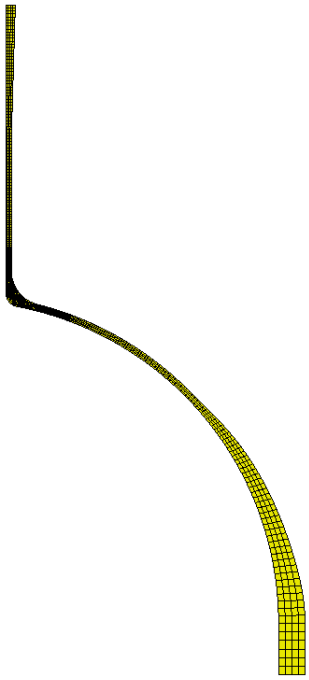

Figure 2: 2D axisymmetric model of the nozzle-to-sphere vessel.

3.1.2 Operating Conditions

The internal surface of the vessel model was subjected to the pressure condition shown in Figure 3. The model was subjected to the temperature condition shown in Figure 4. Since the experiment was carried out for 2.5 years, this analysis considered a total time of 2.5 years.

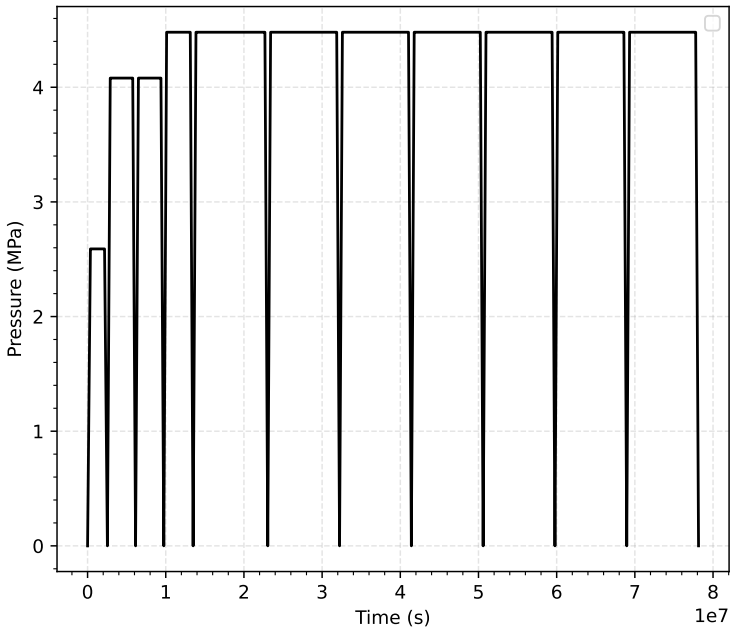

Figure 3: Pressure at the inner surface of the nozzle-to-sphere vessel as a function of time.

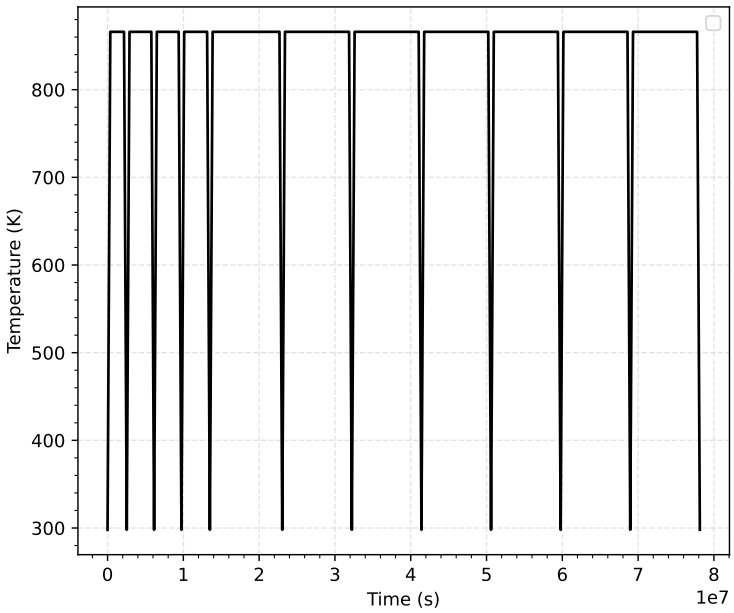

Figure 4: Temperature variation of the nozzle-to-sphere vessel as a function of time.

3.1.3 Results

The analysis results are shown in Figures 5-8. Figure 5 and Figure 6 show the distribution of von Mises stress and inelastic strain, respectively, in the nozzle-to-sphere vessel model at the end of 5 months of operation. Figure 7 and Figure 8 show the variation of maximum von Mises stress and maximum inelastic strain, respectively, in the vessel model with time.

The creep strain time history predicted from the finite element analysis was compared with the experimentally obtained creep time history at location of Ring 2 shown in Figure 1. Figure 8 shows a comparison of the predicted creep strain with the experimental data. Once the component begins to deform inelastically, the predicted creep strain is roughly two times greater than the creep strain measurements from the experiment over much of the duration of the experiment, and then deviates even further late in life. The scatter in experimental data on high-temperature creep response can be quite large, so this discrepancy could be partly due to that, but it also likely reflects a need for further improvements to the constitutive model.

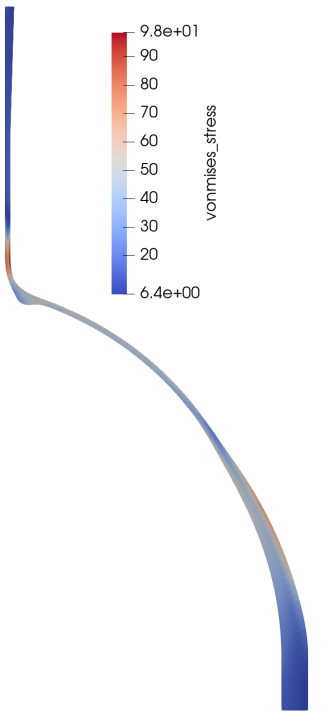

Figure 5: von Mises stress (MPa) distribution in the nozzle-to-sphere vessel at the end of 5 months.

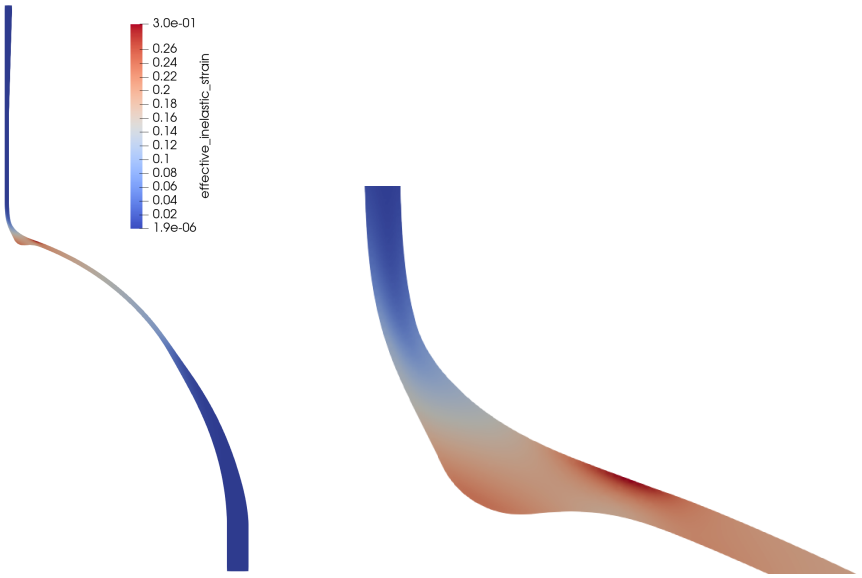

Figure 6: Inelastic strain distribution in the nozzle-to-sphere vessel at the end of 5 months.

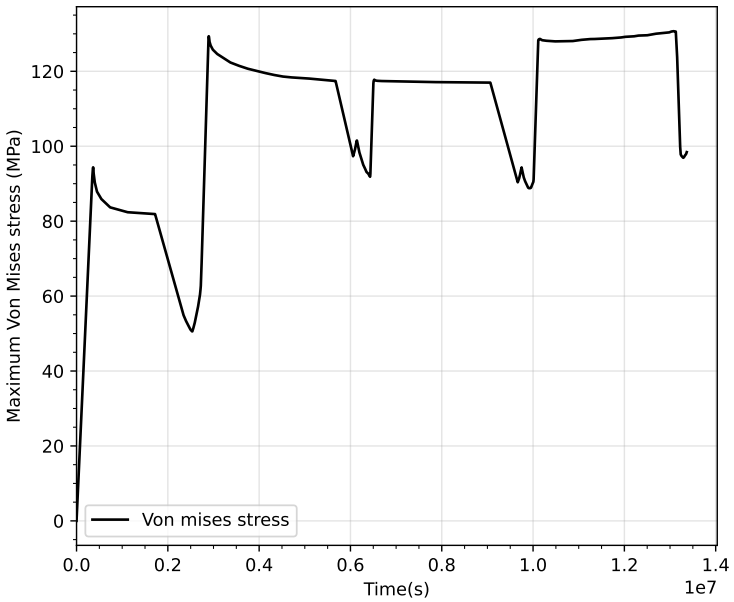

Figure 7: Maximum von Mises stress in the nozzle-to-sphere vessel as a function of time.

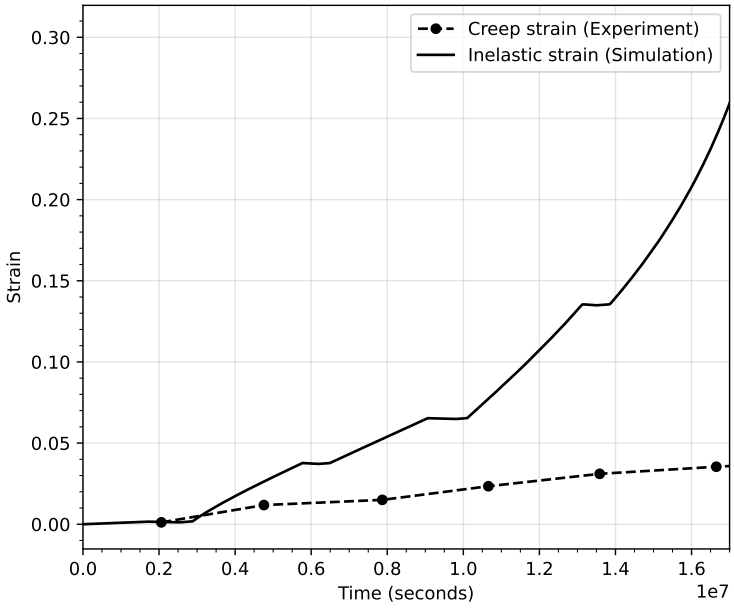

Figure 8: Predicted and measured creep strain in the nozzle-to-sphere vessel as a function of time at Ring 2 (shown in Figure 1) [29].

3.2 Hot Gas Duct Problem

The hot gas duct example problem is based on the design of the hot gas duct component in helium engineering demonstration loop [31]. This design is intended for use in high-temperature gas-cooled reactors. Figure 9 shows the schematic layout of the hot duct.

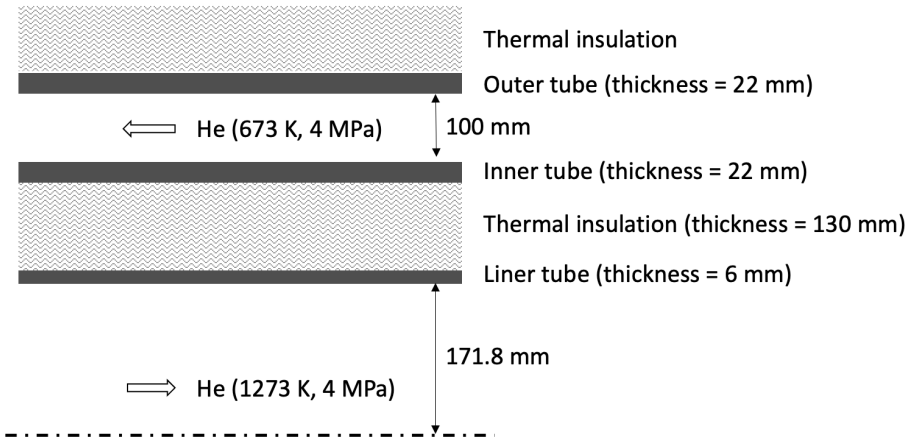

Figure 9: Schematic layout of the hot duct. Modified from Reference [32].

The hot helium gas flows through the liner tube and cool helium gas flows through the channel between the inner and outer tube. The inner tube stays at 673 K during normal operation. At this temperature, the inner tube does not undergo significant creep and therefore creep damage is negligible. However, if there is an accident that breaks the thermal insulation between the inner tube and liner tube, the temperature of the inner tube rises quickly to levels at which creep rate becomes significant. At these elevated temperatures, the inner tube undergoes creep damage.

As soon as the thermal insulation breaks, the control system activates the emergency shutdown, which cools the hot helium to 673 K in 10 hours. This temperature variation with time during an accident is shown in Figure 10. During the accident, the inner tube temperature rises high enough for creep damage to occur. A large number of such accident cycles are simulated to understand the accumulation of creep damage with accidents and to ultimately understand how many such accidents can be tolerated by the inner tube before it fails due to the creep damage.

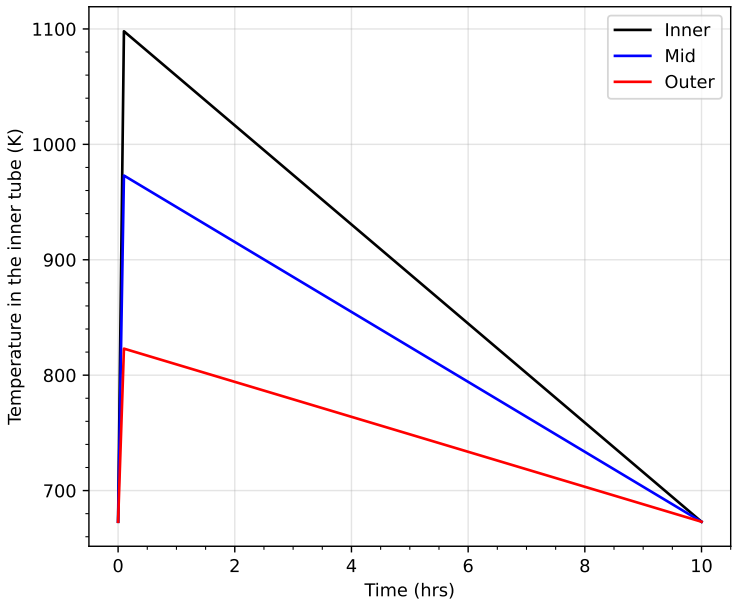

Figure 10: Variation of temperature in the inner tube of the hot duct during the accident and emergency shutdown, based on a transient heat transfer analysis reported in [32].

3.2.1 Geometry Mesh and Material

For this analysis, 2D axisymmetric model was used. The dimensions of the model are shown in Figure 9. The meshed 2D axisymmetric model consists of 500 HEX8 elements, with 50 elements in the radial direction and 10 elements in the axial direction. The inner tube is assumed to be made of Alloy 617, and a NEML model of this material was used for the analysis. The creep model for Alloy 617 is described in section 2.

3.2.2 Operating Conditions

During normal operating conditions, the pressure at the outer surface of the inner tube is kept constant at 4 MPa, and the entire inner tube is at 673 K. The drop in temperature during an accident condition is shown in Figure 10. This variation of temperature in the hot duct is applied as a boundary condition to the model. The temperature distribution during an accident is shown in Figure 11.

The operating temperature cycles are shown in Figure 12. The hot duct was assumed to operate at normal conditions for 1,010 hours (AB) followed by an accident (BC and CD). During an accident, the temperature increases sharply for about 6 minutes (BC) followed by cool down (CD) due to emergency shutdown. The temperature cool-down time was considered to be 10 hours as shown earlier in Figure 10. A total of 27 such cycles of normal operation followed by an accident, during the course of 3.2 years, was considered in the analysis.

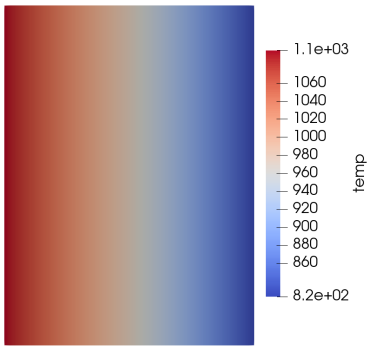

Figure 11: Temperature distribution in the inner tube of the hot duct during an accident.

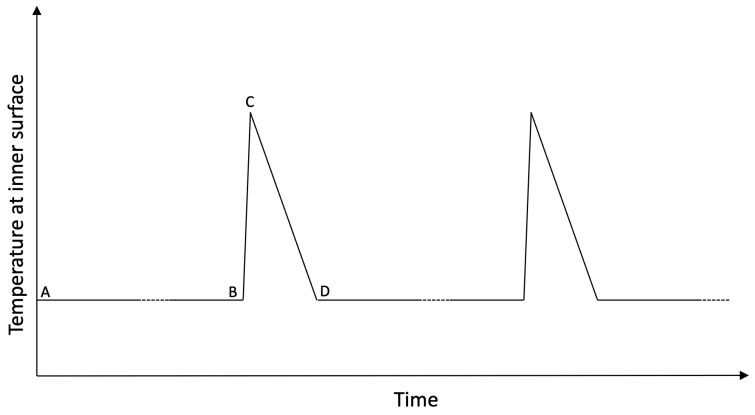

Figure 12: Temperature variation at a location in the inner tube as a function of time. The sharp rise (BC) and drop (CD) in temperature represent temperature variation during the accident situation.

3.2.3 Results

The analysis results are shown in figures 13 to 16. Figure 13 and Figure 14 show the distribution of the von Mises stress and inelastic strain, respectively, in the inner tube cross section of the inner tube at the end of 3.2 years (after 27 cycles). Figure 15 and Figure 16 show the variation of maximum von Mises stress and maximum inelastic strain, respectively, in the inner tube with time.

Figure 16 shows that, during the normal operating conditions, the maximum inelastic strain is nearly constant, while during the accident, when temperature rises in the tube, the creep strain increases rapidly. Thus, a "staircase step" is seen for each of the 27 cycles in the figure.

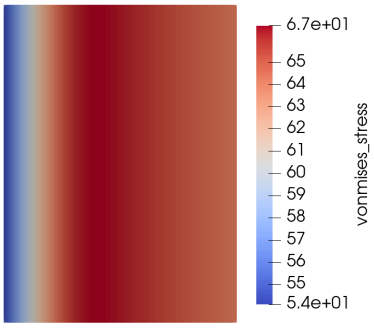

Figure 13: von Mises stress (MPa) distribution in the inner tube cross section at the end of 3.2 years. The radially outward direction corresponds to the horizontal direction (left to right), and the axial direction corresponds to the vertical direction in the page.

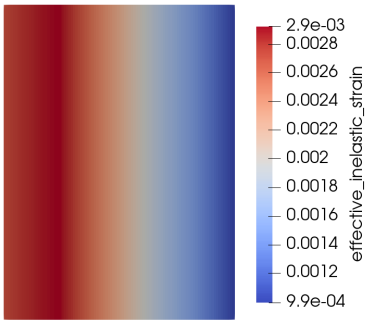

Figure 14: Inelastic strain distribution in the inner tube cross section at the end of 3.2 years. The radially outward direction corresponds to the horizontal direction (left to right), and the axial direction corresponds to the vertical direction in the page.

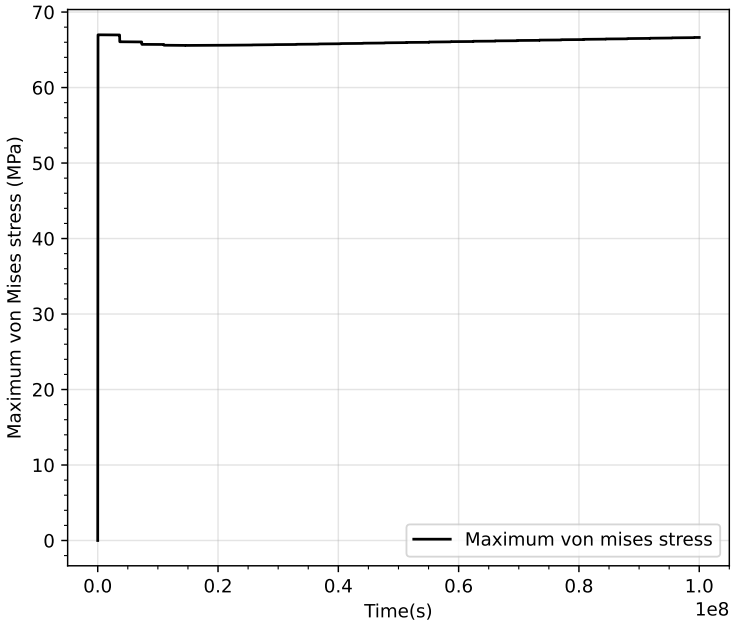

Figure 15: Maximum von Mises stress in the inner tube as a function of time.

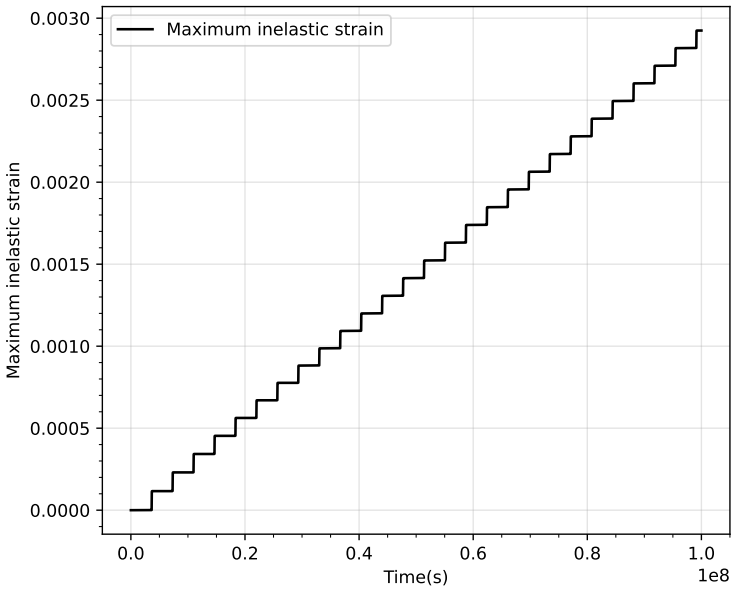

Figure 16: Maximum inelastic strain in the inner tube as a function of time.

3.3 Lateral Pipe Branch Problem

Lateral pipe branches are commonly used in steam pipes in a variety of systems, including nuclear power plants. A representative pipe lateral branch was added to the Grizzly example problems.

3.3.1 Geometry Mesh and Material

This simulation uses the full three dimensional pipe lateral model analyzed in [33] and shown in Figure 17. The mesh for this model, shown in Figure 18, consists of 22,167 HEX8 elements and 32,150 nodes. The main (horizontal) pipe is meshed with three elements along the thickness direction, which gradually transitions to a single element for the branched pipe. The pipe structure is modeled with half symmetry boundary conditions (i.e., zero z-displacement along the cut pipe face normal to the x-y plane).

The nodes on the right end have zero y-displacement, and the x-displacement is fixed on one node to remove rotations about the z-axis. An internal pressure is applied to the inside of the of pipe and the external pressure is set to zero. These boundary conditions approximately model infinitely long pipes with closed ends extending from this junction. The simulations are initialized with a constant internal pressure of 2 MPa and uniform temperature of 550°C.

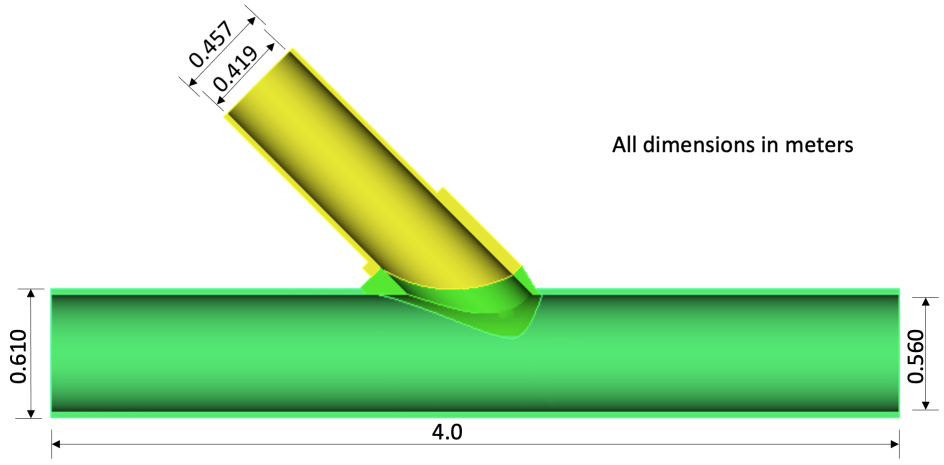

Figure 17: Dimensions of the lateral pipe branch model [33].

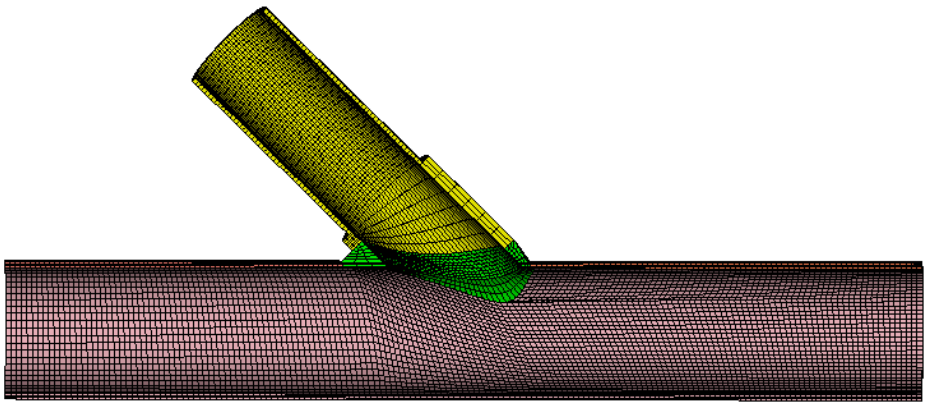

Figure 18: Meshed model of the lateral pipe branch.

3.3.2 Operating Conditions

The pipe branch model is considered to operate at a constant pressure of 2 MPa and temperature of 550 °C for 20 years. Currently, the changes in the temperature and pressure due to shutdowns have not been considered.

3.3.3 Results

The linear elastic von Mises stress, which is the stress field at the start of the creep simulation, is shown in Figure 19. Inelastic strain and von Mises stress histories are shown in Figure 20 for the locations numbered in Figure 19. The maximum elastic von Mises stress is occurs at Location 1. The greatest stress on the exterior of the pipe occurs at Locations 2 and 3. Location 4 is the region of the pipe where the stress field is given by the analytic equation for a thick-walled pipe. The stress at Location 4 is low, and the deformation due to inelastic strain is small. The final von Mises stress after 20 years is shown in Figure 21 where stress relaxation at the joint between the two pipes (Location 1) is reduced from 120 to 70 MPa. Location 1 in the joint region also accumulates the most inelastic strain after 20 years, as shown in Figure 22.

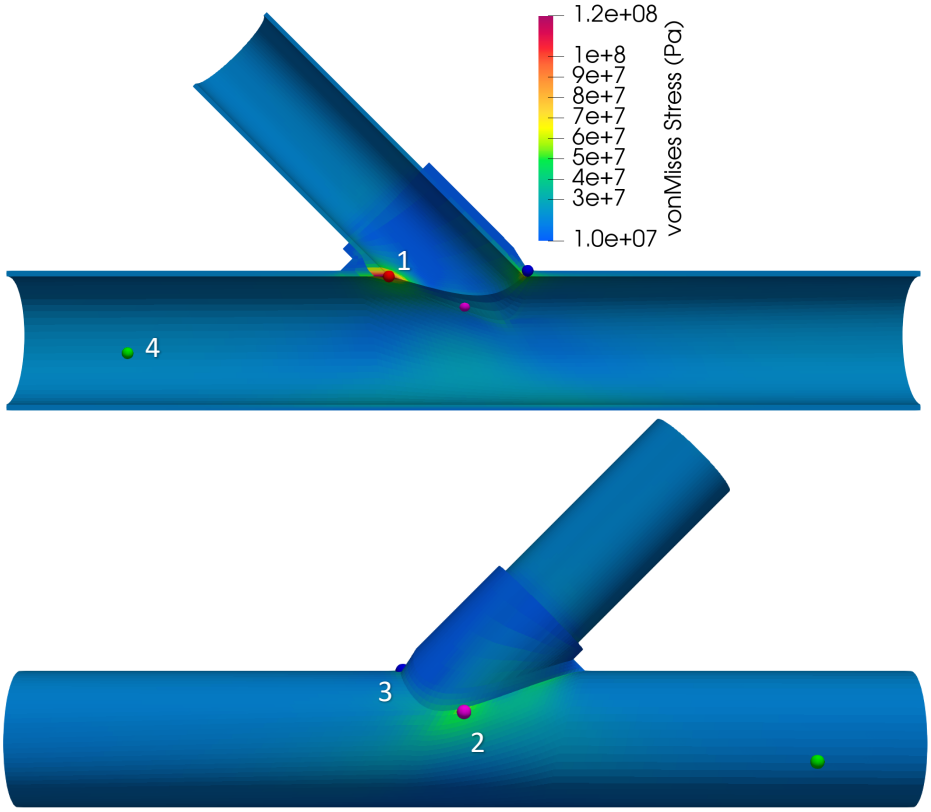

Figure 19: Linear Elastic von Mises stress (MPa) distribution in the pipe lateral pressurized to 2 MPa and temperature 550 °C. Stress and strain histories from Locations 1–4 are shown in Figure 20. Locations 1 and 2 are measured on the pipe interior and Locations 3 and 4 are measured on the pipe exterior.

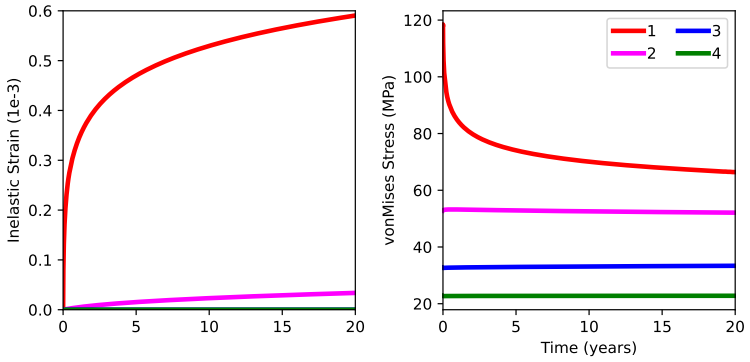

Figure 20: Inelastic strain and von Mises stress in the pipe lateral at locations labeled in Figure 19 as a function of time for P = 2 MPa and T = 550 °C.

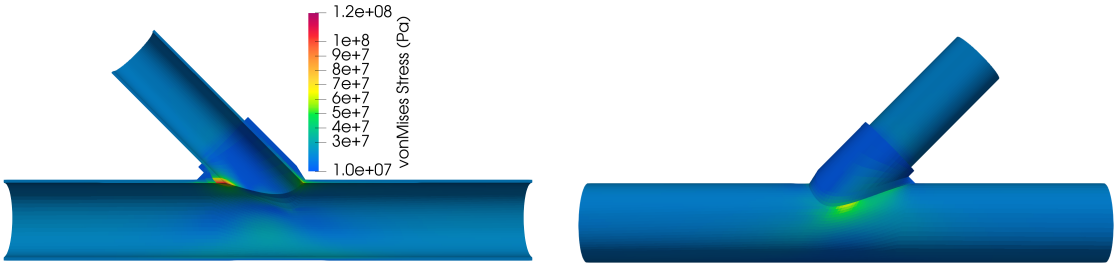

Figure 21: von Mises stress distribution after 20 years for P = 2 MPa and T = 550 °C.

Figure 22: Inelastic strain distribution after 20 years for P = 2 MPa and T = 550 °C.

3.4 Header Problem

This sample problem is of a heat recovery steam generator outlet header given in Reference [32].

3.4.1 Geometry Mesh and Material

A 3D model of the header is used for this example problem. The dimensions of the model are shown in Figure 23. The finite element mesh of this header is shown in Figure 24. The meshed model consists of 21,993 HEX8 elements. The header is considered to be made of Grade 91 steel, and NEML and LAROMANCE Grade 91 material models are used in the analysis. A description of the NEML material model is given in Section 3.3 in Equation 3. Parameters for the NEML model are taken from Table 2 for 600 °C.

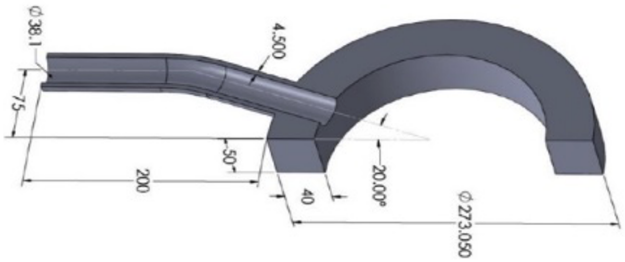

Figure 23: Dimensions of the header model (length units are mm) [32].

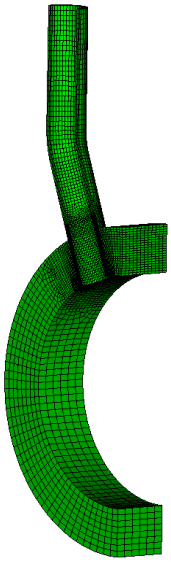

Figure 24: Mesh for the header.

3.4.2 Operating Conditions

The header model is considered to operate at a constant pressure of 7.5 MPa and 600 °C. The operating time of 5 years is considered in this analysis [32].

3.4.3 Results

The analysis results are shown in figures 25 to 27. Figures 25 and 26 show the von Mises stress distribution and the inelastic strain distribution, respectively, in the header at the end of 5 years. Figure 27 shows the von Mises stress and maximum inelastic strain as a function of time for Locations 1 and 2 in Figure 25 (a). The maximum elastic von Mises stress occurs at Location 1. Location 2 provides the stress and strain state for a pressurized thick-walled cylinder.

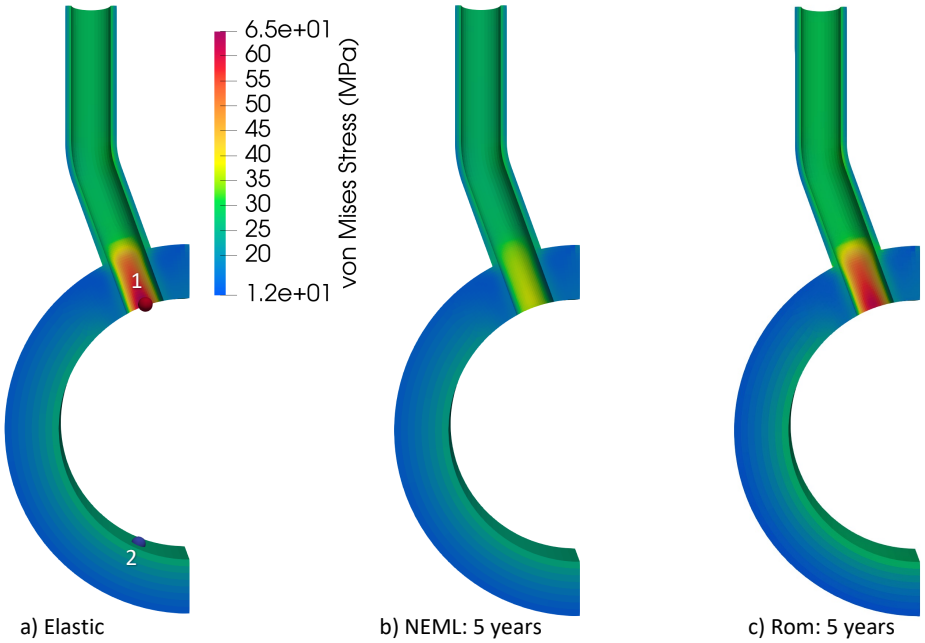

Figure 25: von Mises stress (MPa) distribution in the header pressurized to 7.5 MPa and temperature 600 °C for (a) initial linear elastic properties and the final stress states after 5 years for the (b) NEML and (c) LAROMANCE Grade 91 material models. Stress and strain histories from Locations 1 and 2 in (a) are shown in Figure 27.

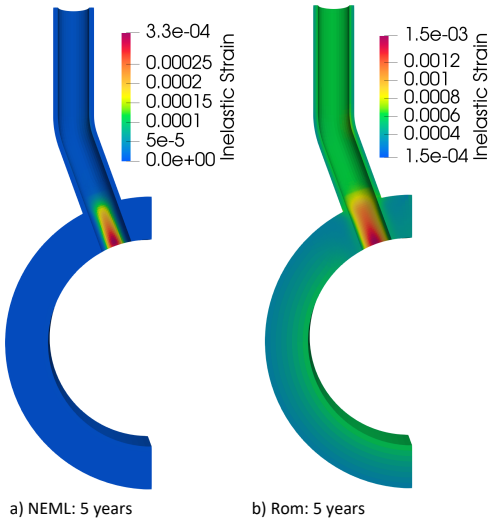

Figure 26: Inelastic strain distribution in the header after 5 years pressurized to 7.5MPa and temperature 600 °C for the (a) NEML and (b) LAROMANCE Grade 91 material models.

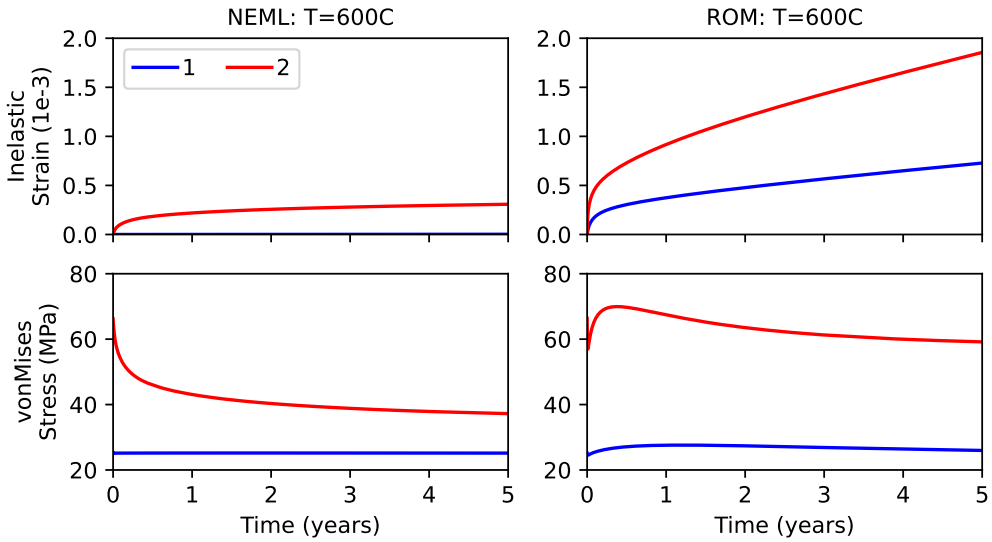

Figure 27: Inelastic strain and von Mises stress in the header at Locations 1 and 2 in Figure 25 as a function of time for the NEML (left column) and LAROMANCE (right column) Grade 91 models for P=7.5 MPa and T=600 °C.

3.5 End Plate Problem

An end plate is used for the end closure of a boiler steam header. The end plate model used in this analysis is based on the ASME CC2697 [34] design rules. This geometry is one of the three examples that were created by the ASME Subgroup on Design for Section I of the ASME Boiler and Pressure Vessel Code for identifying the requirements of a ASME code case under review for incorporation into Section I. This problem has been added as an example to the Grizzly code.

3.5.1 Geometry Mesh and Material

A 2D axisymmetric model of the end plate is used for this example problem. The dimensions and mesh of the endplate model are shown in Figure 28. Further details on dimensions of this part can be found in Reference [34]. The meshed model consists of 9,937 HEX8 elements.

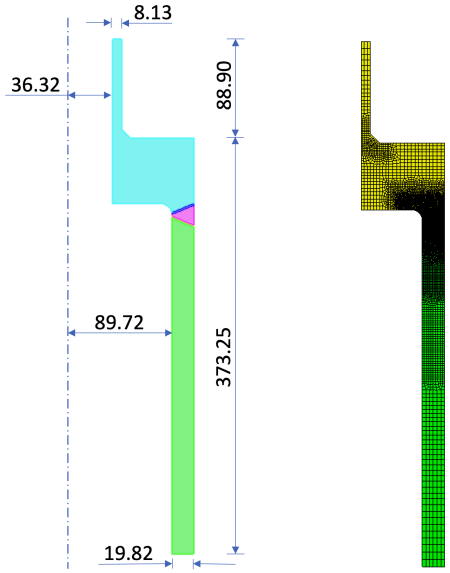

Figure 28: Dimensions and mesh for the end plate (length units are mm).

3.5.2 Operating Conditions

The end plate is considered to operate at a pressure of 15.5 MPa and temperature of 550 °C. The operating time is considered to be 200,000 hours ($\approx$ 22.8 years) in the analysis. The Grade 91 steel is assumed to be the material for the end plate problem, and a NEML model of this material was used for the analysis. The creep model used for this material is described in section 2.

3.5.3 Results

The analysis results are shown in figures 29 to 32. Figure 29 and Figure 30 show the distribution of von Mises stress and inelastic strain, respectively, in the end plate model at the end of 22.8 years of operation. Figure 31 and Figure 32 show the variation of maximum von Mises stress and maximum inelastic strain, respectively, in the end plate model with time.

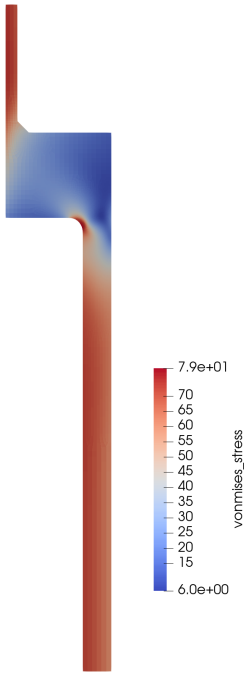

Figure 29: von Mises stress (MPa) distribution in the end plate.

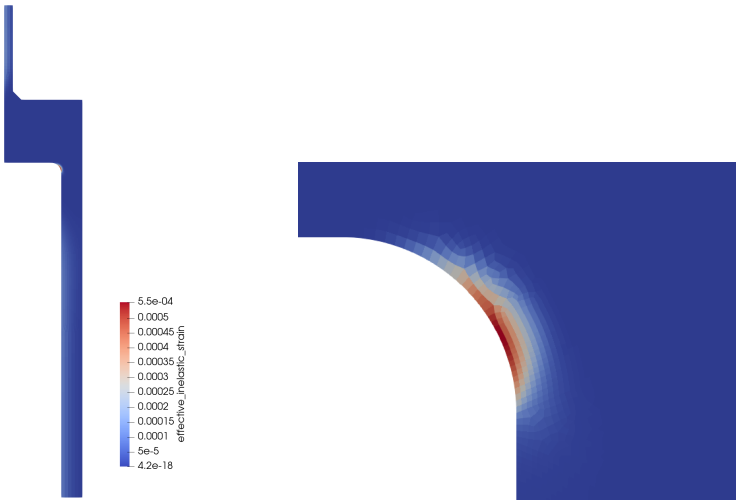

Figure 30: Inelastic strain distribution in the end plate.

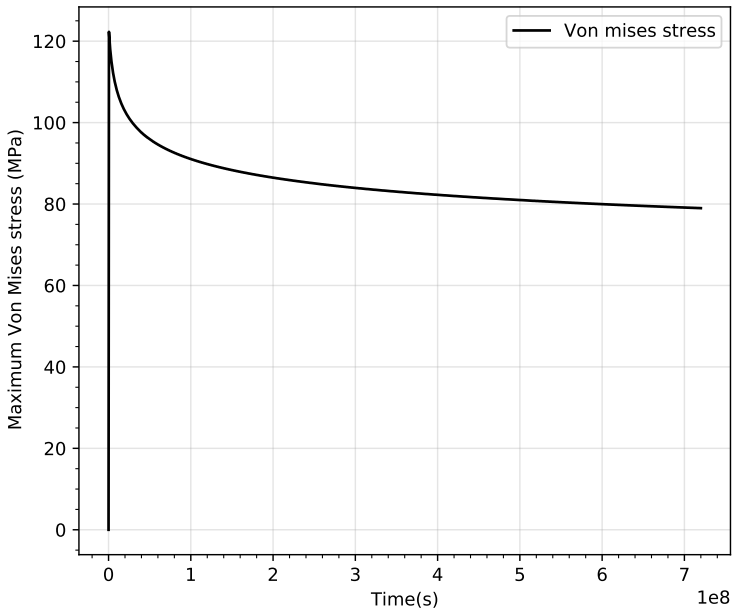

Figure 31: Maximum von Mises stress in the end plate as a function of time.

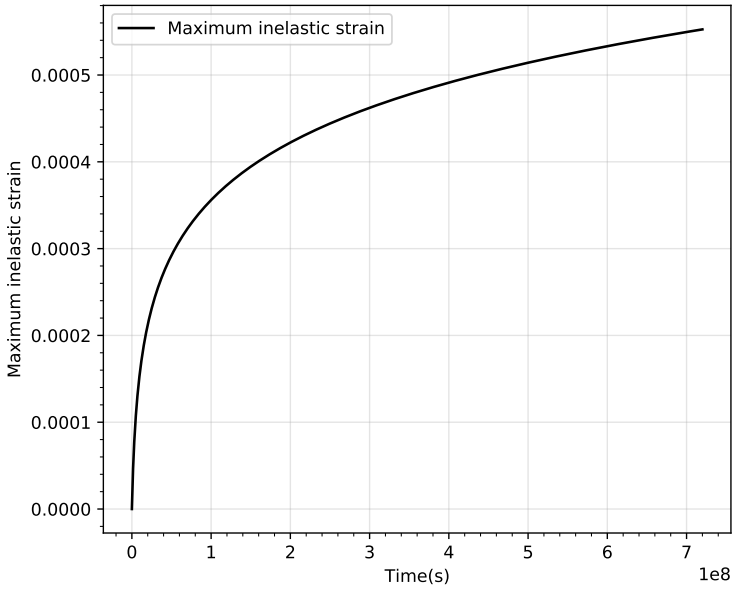

Figure 32: Maximum inelastic strain as a function of time in the end plate.

3.6 Materials Comparison

In addition to the set of test cases on component geometries, a set of problems that capture the creep response of the available material models under the conditions experienced in a uniaxial creep test was developed. These tests apply constant unixaial loading at a variety of magnitudes and temperatures to assist in understanding the material response.

3.6.1 Geometry Mesh and Materials

The study was performed using a single element with unit dimensions as shown in Figure 33. Alloy 617, Grade 91 steel, 304 stainless steel, Grade 22 steel, and 316 stainless steel were considered for the study. The creep models for these materials are discussed in section 2.

3.6.2 Test Conditions

Constant tensile stress was applied in single direction over 22 years (200,000 hours). Different cases of tensile stress magnitudes ranging from 40 to 90 MPa were analyzed. A constant temperature of 823 K was considered during the test. For Grade 91 steel additional tests at 873 K were simulated for comparing the creep response of the material at 823 and 873 K.

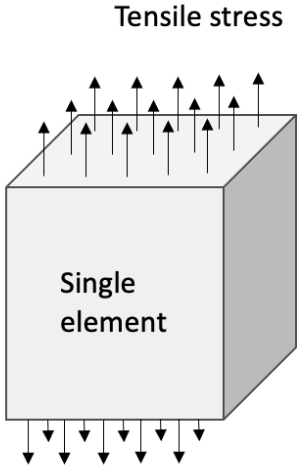

Figure 33: Schematic of the simulated tensile creep test.

3.6.3 Results

The results from the study are shown in Figures 34 to 37. Figures 34 to 36 show the variation of inelastic strain as a function of time for stress levels ranging from 40 to 90 MPa. Figure 37 shows a comparison of the creep response of Grade 91 steel at two temperatures (823 and 873 K) at tensile stress levels of 40, 60, and 80 MPa.

Under the conditions tested (at 550 °C), the ranking of these alloys from the lowest to highest creep resistance is generally: Grade 22 alloy, 304 stainless steel, 316 stainless steel, Grade 91 alloy, and Alloy 617.

This behavior generally holds across all stress levels, although at the highest and lowest stress levels tested, 316 stainless steel has slightly higher creep resistance than Grade 91 alloy.

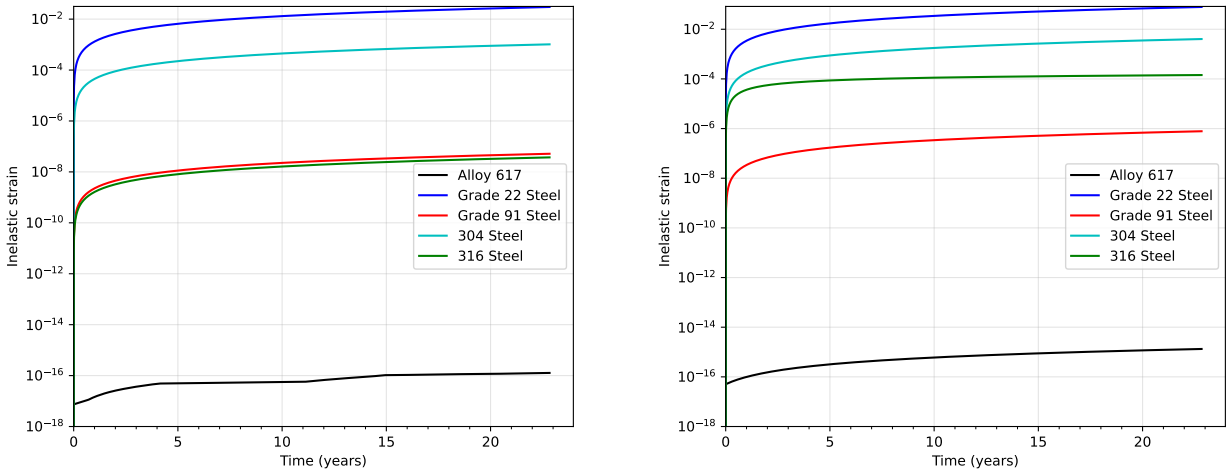

Figure 34: Inelastic creep strain as a function of time at a constant stress of 40 MPa (left) and 50 MPa (right) for the simulated uniaxial tensile creep test.

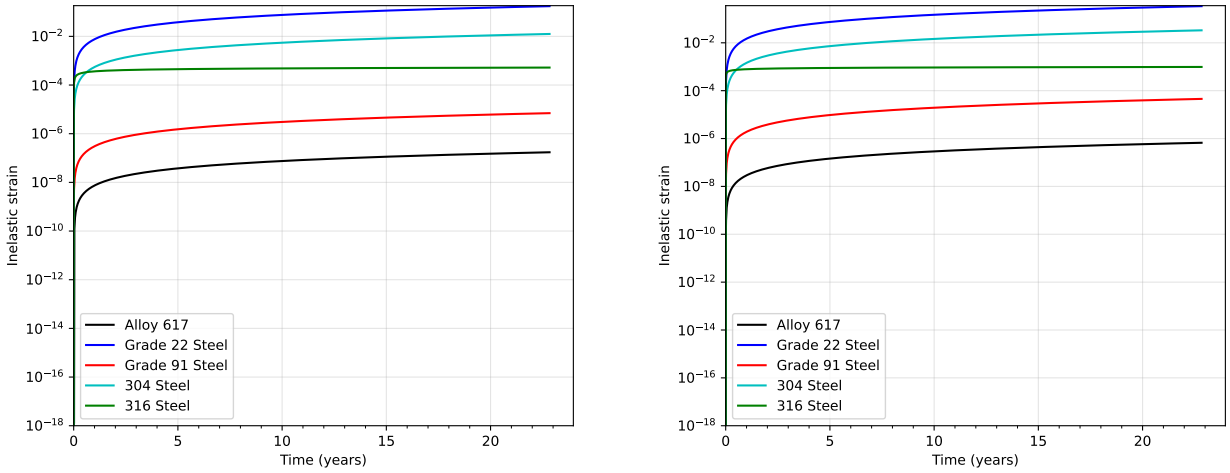

Figure 35: Inelastic creep strain as a function of time at constant stress of 60 MPa (left) and 70 MPa (right) for the simulated uniaxial tensile creep test.

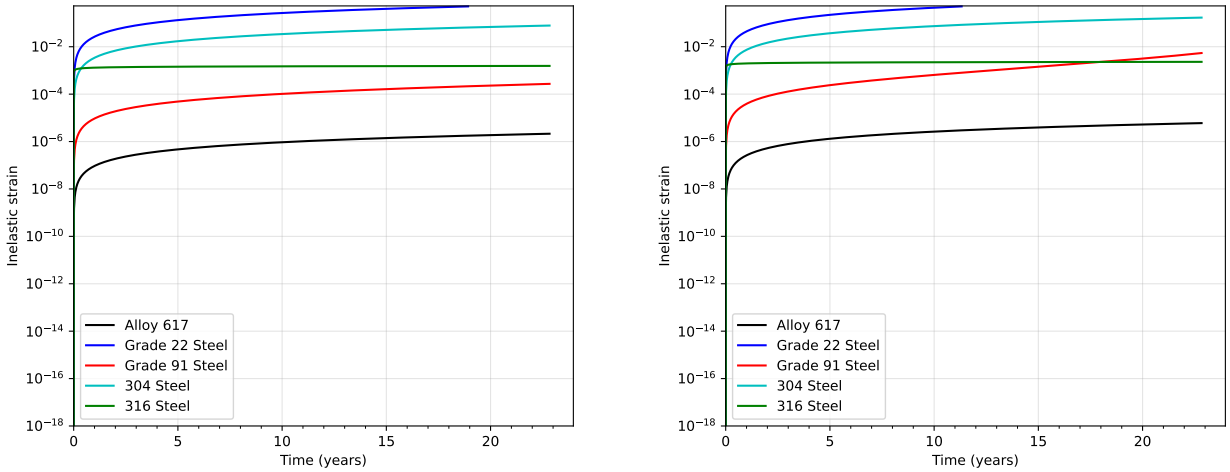

Figure 36: Inelastic creep strain as a function of time at constant stress of 80 MPa (left) and 90 MPa (right) for the simulated uniaxial tensile creep test.

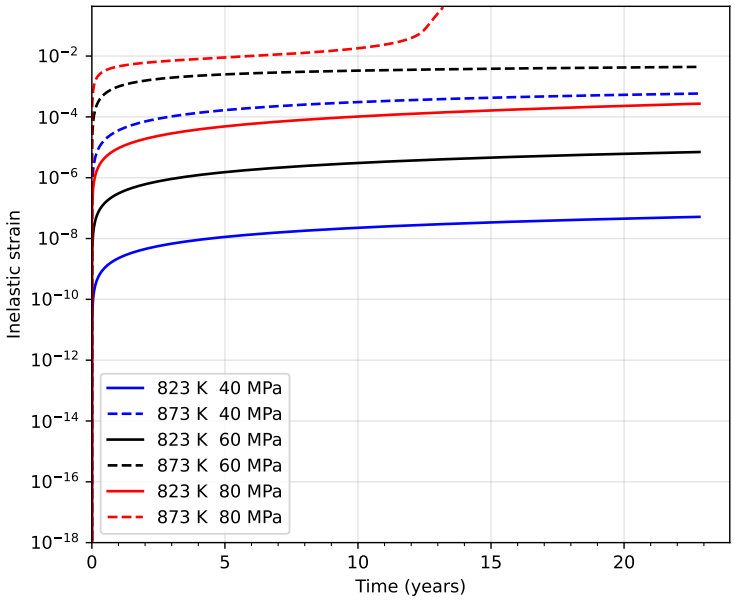

Figure 37: Inelastic strain as a function of time for the Grade 91 steel at different temperatures and tensile load levels.

4 SUMMARY AND FUTURE WORK

An initial version of a test suite for high-temperature alloy responses has been developed in Grizzly. This test suite includes problems that test code behavior on practical models with five different geometries, using both 2D axisymmetric and 3D geometric representations, and tests four different materials relevant to high-temperature nuclear applications. In addition, this test suite includes a set of simple uniaxial creep test cases to improve the understanding of the material response predicted by these models.

Overall, the numerical performance of the code on these test cases is very good. All of these problems require small iteration counts for convergence. Some of the test cases require the use of a parallel direct solver, while others can be used with a more scalable iterative solver. Because there is relatively little experimental data on component response, unfortunately most of these test cases do not have experimental data, so they are primarily useful for examples, performance testing, and testing new features and models in the future.

Major areas of future development on this test suite in the near term include testing optimal settings for efficient and accurate time stepping, testing new surrogate material models as they become available, and testing damage modeling approaches. One modeling feature that could improve one of the cases in this test suite is a constraint that can maintain a planar surface that is not oriented with one of the Cartesian axes. This would be useful for the free end of the smaller pipe in the lateral pipe problem, which is oriented at a 45° angle to the main pipe.

In the longer term, as data on the response of components constructed of these alloys under high-temperatures become available, especially with damage data, it would be of great interest to expand this test suite to include that type of problem. In addition, adding additional test cases with problems that have unique geometries, exercise other modeling features, or expand the set of regimes of material behavior would also be of interest.

REFERENCES

[1] B. W. Spencer, W. M. Hoffman, S. Biswas, W. Jiang, A. Giorla, and M. A. Backman, "Grizzly and BlackBear: Structural component aging simulation codes," *Nuclear Technology*, vol. 207, pp. 981–1003, Apr. 2021.

[2] G. Was, D. Petti, S. Ukai, and S. Zinkle, "Materials for future nuclear energy systems," *Journal of Nuclear Materials*, vol. 527, p. 151837, Dec. 2019.

[3] L. B. Munday, S. L. Dhulipala, A. Casagranda, S. A. Pitts, B. W. Spencer, L. Capolungo, A. E. Tallman, M. A. Kumar, C. Matthews, M. C. Messner, and A. E. Chakraborty, "Multiscale-informed modeling of high temperature component response with uncertainty quantification," Tech. Rep. INL/EXT-20-59795, Idaho National Laboratory, August 2020.

[4] L. B. Munday, J. H. Ke, A. Jain, B. W. Spencer, W. M. Hoffman, and D. Schwen, "Grizzly development for light water reactor and advanced reactor applications in Fiscal Year 2021," Tech. Rep. INL/EXT-21-64574, Idaho National Laboratory, September 2021.

[5] C. J. Permann, D. R. Gaston, D. Andrš, R. W. Carlsen, F. Kong, A. D. Lindsay, J. M. Miller, J. W. Peterson, A. E. Slaughter, R. H. Stogner, and R. C. Martineau, "MOOSE: Enabling massively parallel multiphysics simulation," *SoftwareX*, vol. 11, p. 100430, Jan. 2020.

[6] A. E. Slaughter, C. J. Permann, J. M. Miller, B. K. Alger, and S. R. Novascone, "Continuous integration, in-code documentation, and automation for nuclear quality assurance conformance," *Nuclear Technology*, vol. 207, pp. 923–930, Jan. 2021.

[7] D. M. Perez, R. L. Williamson, S. R. Novascone, R. J. Gardner, K. A. Gamble, A. T. Rice, G. Pastore, J. D. Hales, and B. W. Spencer, "Assessment of BISON: A nuclear fuel performance analysis code, BISON Release 1.1," Tech. Rep. INL/MIS-13-30314 Rev. 1, Idaho National Laboratory, October 2014.

[8] R. Williamson, K. Gamble, D. Perez, S. Novascone, G. Pastore, R. Gardner, J. Hales, W. Liu, and A. Mai, "Validating the BISON fuel performance code to integral LWR experiments," *Nuclear Engineering and Design*, vol. 301, pp. 232–244, May 2016.

[9] B. W. Spencer, W. M. Hoffman, S. Biswas, and A. Jain, "Assessment of Grizzly capabilities for reactor pressure vessels and reinforced concrete structures," Tech. Rep. INL/EXT-20-59941, Idaho National Laboratory, September 2020.

[10] W. M. Hoffman and B. W. Spencer, "Benchmarking of probabilistic fracture mechanics models in Grizzly," Tech. Rep. TLR-RES/DE/REB-2021-07, INL/EXT-21-62199, Idaho National Laboratory, June 2021.

[11] "NEML — Nuclear Engineering Material model Library."

[12] A. O. Schaefer, *The Generation of Isochronous Stress-Strain Curves*. American Society of Mechanical Engineers, 1972.

[13] M. Messner and T.-L. Sham, "Isochronous stress-strain curves for Alloy 617," in *Pressure Vessels and Piping Conference*, vol. 58929, p. V001T01A062, American Society of Mechanical Engineers, 2019.

[14] A. Chakraborty and M. Messner, "Bayesian analysis for estimating statistical parameter distributions of elasto-viscoplastic material models," *Probabilistic Engineering Mechanics*, vol. 66, p. 103153, 2021.

[15] P. Perzyna, "Fundamental Problems in Viscoplasticity," *Advances in Applied Mechanics*, vol. 9, no. C, pp. 243–377, 1966.

[16] J. L. Chaboche, "A review of some plasticity and viscoplasticity constitutive theories," *International Journal of Plasticity*, vol. 24, pp. 1642–1693, oct 2008.

[17] F. A. Leckie and D. R. Hayhurst, "Constitutive equations for creep rupture," *Acta Metallurgica*, vol. 25, no. 9, pp. 1059–1070, 1977.

[18] W. Wen, L. Capolungo, A. Patra, and C. N. Tomé, "A physics-based crystallographic modeling framework for describing the thermal creep behavior of Fe-Cr alloys," *Metallurgical and Materials Transactions A*, vol. 48, no. 5, pp. 2603–2617, 2017.

[19] M. Basirat, T. Shrestha, G. Potirniche, I. Charit, and K. Rink, "A study of the creep behavior of modified 9Cr–1Mo steel using continuum-damage modeling," *International Journal of Plasticity*, vol. 37, pp. 95–107, 2012.

[20] A. E. Tallman, M. A. Kumar, A. Castillo, W. Wen, L. Capolungo, and C. N. Tomé, "Data-driven constitutive model for the inelastic response of metals: Application to 316H steel," *Integrating Materials and Manufacturing Innovation*, vol. 9, no. 4, pp. 339–357, 2020.

[21] M. Messner and T.-L. Sham, "Reference constitutive model for Alloy 617 and 316H stainless steel for use with the ASME Division 5 design by inelastic analysis rules," tech. rep., Argonne National Lab.(ANL), Argonne, IL (United States), 2021.

[22] Y. Estrin and H. Mecking, "A unified phenomenological description of work hardening and creep based on one-parameter models," *Acta metallurgica*, vol. 32, no. 1, pp. 57–70, 1984.

[23] U. Kocks, "Realistic constitutive relations for metal plasticity," *Materials Science and Engineering: A*, vol. 317, no. 1-2, pp. 181–187, 2001.

[24] V.-T. Phan, M. Messner, and T.-L. Sham, "A unified engineering inelastic model for 316h stainless steel," in *Pressure Vessels and Piping Conference*, vol. 58929, p. V001T01A040, American Society of Mechanical Engineers, 2019.

[25] A. Chakraborty, M. C. Messner, and T.-L. Sham, "A minimum creep rate for 2-1/4cr-1mo steel consistent with the asme section iii, division 5 rules," *Journal of Pressure Vessel Technology*, vol. 143, no. 4, 2021.

[26] S. Balay, S. Abhyankar, M. F. Adams, S. Benson, J. Brown, P. Brune, K. Buschelman, E. M. Constantinescu, L. Dalcin, A. Dener, V. Eijkhout, W. D. Gropp, V. Hapla, T. Isaac, P. Jolivet, D. Karpeev, D. Kaushik, M. G. Knepley, F. Kong, S. Kruger, D. A. May, L. C. McInnes, R. T. Mills, L. Mitchell, T. Munson, J. E. Roman, K. Rupp, P. Sanan, J. Sarich, B. F. Smith, S. Zampini, H. Zhang, H. Zhang, and J. Zhang, "PETSc Web page," 2022.

[27] X. S. Li, "An overview of SuperLU," *ACM Transactions on Mathematical Software*, vol. 31, pp. 302–325, Sept. 2005.

[28] V. E. Henson and U. M. Yang, "BoomerAMG: A parallel algebraic multigrid solver and preconditioner," *Applied Numerical Mathematics*, vol. 41, pp. 155–177, Apr. 2002.

[29] J. Corum and R. Battiste, "Predictability of long-term creep and rupture in a nozzle-to-sphere vessel model," *J. Pressure Vessel Technol.*, vol. 115, pp. 122–127, 1993.

[30] T. D. Blacker, S. J. Owen, M. L. Staten, W. R. Quadros, B. Hanks, B. W. Clark, R. J. Meyers, C. Ernst, K. Merkley, R. Morris, *et al.*, "CUBIT geometry and mesh generation toolkit 15.1 user documentation," tech. rep., Sandia National Lab.(SNL-NM), Albuquerque, NM (United States), 2016.

[31] N. Izawa, Y. Inagaki, T. Tanaka, M. Hishida, H. Shimomura, and Y. Okamoto, "An overview of helium engineering demonstration loop (hendel) 1982," 1982.

[32] B. Barua, M. Messner, Y. Wang, T.-L. Sham, and R. Jetter, "Draft rules for Alloy 617 creep-fatigue design using an EPP+ SMT approach," tech. rep., Argonne National Lab.(ANL), Argonne, IL (United States), 2021.

[33] D. Dewees, J. A. Mann III, C. Nadarajah, M. Messner, B. Hantz, and D. Andersen, "Comparison of candidate steady loading elevated temperature design-by-analysis methods," in *Pressure Vessels and Piping Conference*, vol. 85321, p. V002T03A065, American Society of Mechanical Engineers, 2021.

[34] M. Cooch, D. Dewees, and G. Komora, "Comparison of header flat end plate designs for operation in the creep range," in *Pressure Vessels and Piping Conference*, vol. 50411, p. V005T12A003, American Society of Mechanical Engineers, 2016.